Terra Nova

doi: 10.1111/ter.12079

P–T–t estimation of deformation in low-grade quartz-feldspar-bearing rocks using thermodynamic modelling and $^{40}Ar/^{39}Ar$ dating techniques: example of the Plan-de-Phasy shear zone unit (Briançonnais Zone, Western Alps)

Pierre Lanari,[1] Yann Rolland,[2] Stéphane Schwartz,[3] Olivier Vidal,[3] Stéphane Guillot,[3] Pierre Tricart[3] and Thierry Dumont[3]

[1]*Institute of Geological Sciences, University of Bern, Baltzerstrasse 3, Bern CH-3012, Switzerland;* [2]*Géoazur, UMR7329-CNRS, UNS, 250 rue Albert Einstein Sophia Antipolis, Valbonne 06560, France;* [3]*ISTerre, University of Grenoble 1, CNRS, 1381 rue de la Piscine 38041, Grenoble, France*

ABSTRACT

Pressure–Temperature–time (*P–T–t*) estimates of the syn-kinematic strain at the peak-pressure conditions reached during shallow underthrusting of the Briançonnais Zone in the Alpine subduction zone was made by thermodynamic modelling and $^{40}Ar/^{39}Ar$ dating in the Plan-de-Phasy unit (SE of the Pelvoux Massif, Western Alps). The dated phengite minerals crystallized syn-kinematically in a shear zone indicating top-to-the-N motion. By combining X-ray mapping with multi-equilibrium calculations, we estimate the phengite crystallization conditions at 270 ± 50 °C and 8.1 ± 2 kbar at an age of 45.9 ± 1.1 Ma. Combining this *P–T–t* estimate with data from the literature allows us to constrain the timing and geometry of Alpine continental subduction. We propose that the Briançonnais units were scalped on top of the slab during ongoing continental subduction and exhumed continuously until collision.

Terra Nova, 26, 130–138, 2014

Introduction

Estimation of burial and exhumation rates, and subsequent building of consistent geodynamic models of continental subduction processes and orogenic evolution, are based on our knowledge of Pressure–Temperature–time (*P–T–t*) paths recorded by the different units across mountain belts (e.g. Ernst, 1988; Rolland *et al.*, 2012). This goal can be easily achieved in well-equilibrated high-grade metamorphic rocks for which several methods are available to estimate *P–T* conditions, such as pseudosections (e.g. Connolly, 2005), and dates, such as $^{40}Ar/^{39}Ar$ or U-Th-Pb (McDougall and Harrison, 1988). In contrast, estimating *P–T* conditions using classical approaches is challenging for most low-grade ($T < 300$ °C) quartzo-feldspathic and pelitic rocks, because they consist of high variance phase assemblages (quartz, K-white mica (KWM) and chlorite) with large stability fields. *P–T* conditions of HP-LT metapelites and of low-grade quartzo-feldspathic rocks may be estimated from the composition of chlorite and KWM using a multi-equilibrium approach (Vidal and Parra, 2000; Cantarero *et al.*, 2013). This approach has been combined with X-ray compositional mapping to depict complex *P–T–d* histories of meta-sandstone samples (Lanari *et al.*, 2012).

Furthermore, KWM can be dated using the $^{40}Ar/^{39}Ar$ dating method. As the closure temperature of KWM is higher than 400 °C (Harrison *et al.*, 2009), dating of low-grade KWM (<400 °C) provides information on the timing of crystallization or of hydrothermal reset (Tartèse *et al.*, 2011). As deformation provides the energy required for grain nucleation under varying *P* and *T* conditions (Vidal *et al.*, 2006), it should thus be possible to determine the age of KWM crystallization related to deformation events in low-temperature shear zones (Kirschner *et al.*, 1996; Rolland *et al.*, 2009; Sanchez *et al.*, 2011). The scope of this study is to test this possibility on a selected sample from the Briançonnais Zone of the French Western Alps (Fig. 1), which has been affected by Alpine continental subduction. The selected sample comes from a small tectonic slice of KWM-bearing gneiss known as the 'Plan-de-Phasy granite' pinched in the Briançonnais Frontal Thrust (Kerckhove and Piboule, 1999), which recorded a top-to-the-W tectonic motion during the Early Oligocene collision stage (Dumont *et al.*, 2012).

Correspondence: Dr Pierre Lanari, Institute of Geological Sciences, University of Bern, Baltzerstrasse 3, Bern CH-3012, Switzerland. Tel.: +41 031 631 87 61; fax: +41 031 631 48 43; e-mail: pierre.lanari@geo.unibe.ch

Geological setting

In the Western Alps, the internal zones are made of a stack of oceanic and continental units recording an eastward increase in metamorphic conditions (Rolland *et al.*, 2000; Goffé *et al.*, 2004; Gabalda *et al.*, 2009; Schwartz *et al.*, 2009; Lanari *et al.*, 2012; Gasco *et al.*, 2013). From top to bottom (i) unmetamorphosed obducted (Chenaillet) ophiolite rests upon (ii) the Queyras 'Schistes lustrés', which represent a fossil sedimentary accretionary wedge developed under blueschist facies conditions during subduction of the Tethys Ocean (Agard *et al.*, 2002), structurally above (iii) the eclogitic Monviso ophiolites corresponding to

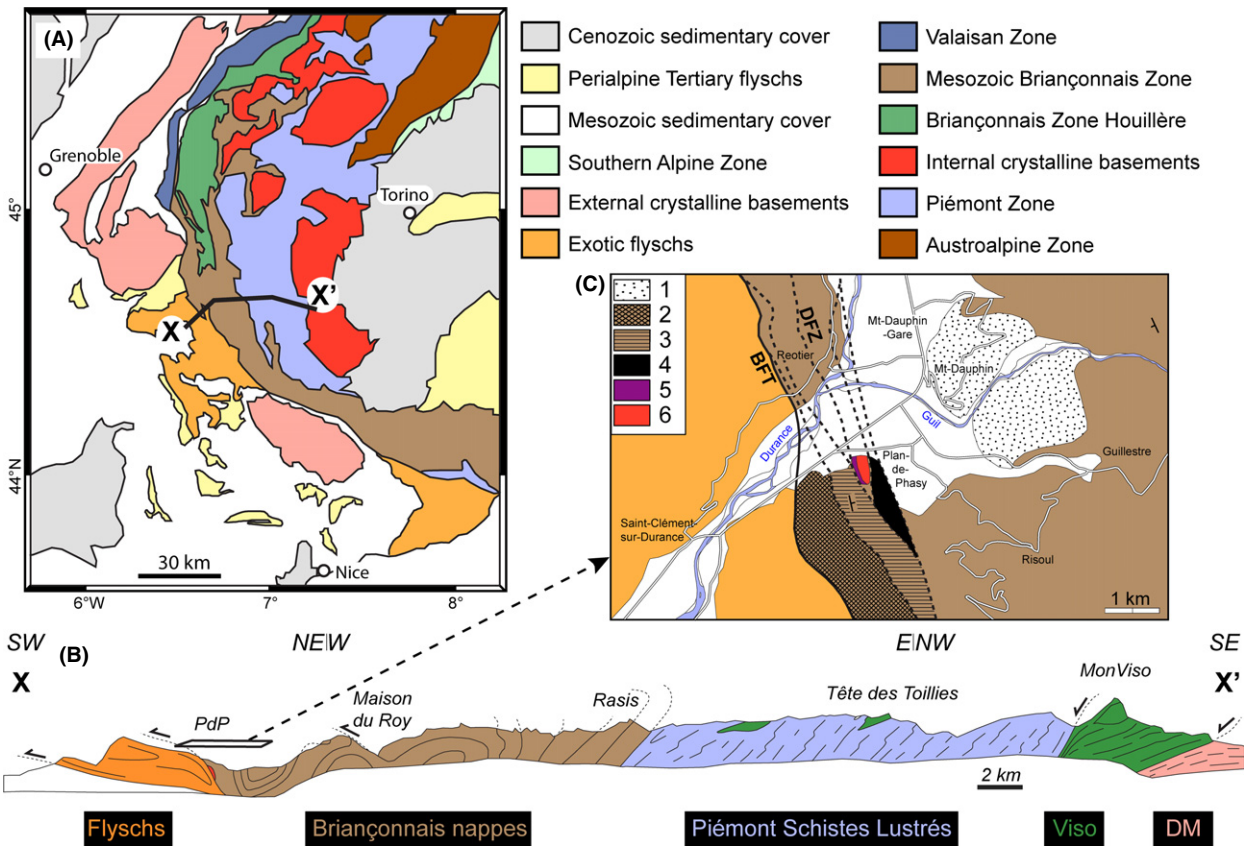

Fig. 1 Geological framework including (A) a schematic map of the Western Alps modified after Bousquet *et al.* (2008) and Dumont *et al.* (2012). (B) Section across the internal zones modified from Lardeaux *et al.* (2006) and Tricart and Schwartz (2006). (C) Detailed map of the Guillestre – Plan-de-Phasy area. 1, Quaternary conglomerates; 2, Eocene 'Flysch noir'; 3, Triassic marble; 4, Triassic Gypsum; 5, Permo-Triassic metasediments; 6 and PdP, Plan-de-Phasy 'granite' basement. BFT, Briançonnais Frontal Thrust (bold line); DFZ Durance Fault Zone (dashed lines).

the deep subduction channel (Schwartz *et al.*, 2001; Angiboust *et al.*, 2012). Metamorphic conditions preserved in each unit have been used to infer the palaeo-thermal gradient (5–8 °C) of the subduction (Lardeaux *et al.*, 2006). Structurally below, (iv) the Briançonnais zone crops out as tectonic windows (Fig. 1). Close to Guillestre, the Upper Briançonnais Zone is made of a stack of late Palaeozoic to Mesozoic sediments that have been affected by greenschist facies conditions (275 ± 23 °C and 5.9 ± 1.7 kbar) during Alpine metamorphism (Caby, 1996; Lanari *et al.*, 2012).

The Plan-de-Phasy unit (Fig. S1) is a 300-m wide highly deformed and recrystallized gneiss slice exhibiting top-to-the-N (D1) and W (D2) sense of shear, surrounded by Permian to Triassic metasediments and gypsum lenses pinched in the Briançonnais Frontal Thrust (Tricart, 1984). This formerly ductile shear zone is reactivated by the extensional-strike slip Durance Fault Zone (Tricart *et al.*, 1996) in more brittle conditions (D3).

Analytical methods and mineral chemistry

Oriented samples were collected in the Plan-de-Phasy unit. The alpine metamorphic assemblage is made of KWM, chlorite and quartz (Fig. 2A). Magmatic-related K-feldspars, plagioclase, rutile, apatite and Fe-oxide minerals were intensely altered and partially recrystallized during alpine deformation (see below). Ductile deformation of quartz and brittle fragmentation of K-feldspars are typical of deformation in the greenschist facies at *c.* 300 °C (Stipp *et al.*, 2002). Two generations of metamorphic minerals were identified using structural and chemical criteria: (1) multi-mm KWM grains crystallized along the S1 schistosity (dashed lines and circles in Fig. 2A, D respectively) during top-to-the-N shearing; and (2) KWM grains sheared during a top-to-the-W deformation event and mm-size chlorite crystallized along S2 schistosity planes (black lines and triangles in Fig. 2A, D respectively).

We selected a small area (1100 × 560 μm^2) in which S1 and S2 are present with chlorite in a S2 zone of fluid impregnation rich in hydrothermal chlorite (Fig. 2B). This area was chemically mapped at the Institute of Earth and Environmental Sciences, Potsdam University using a JEOL JXA-8200 electron microprobe. Analytical conditions for the mapping were 15 KeV accelerating voltage, 100 nA specimen current

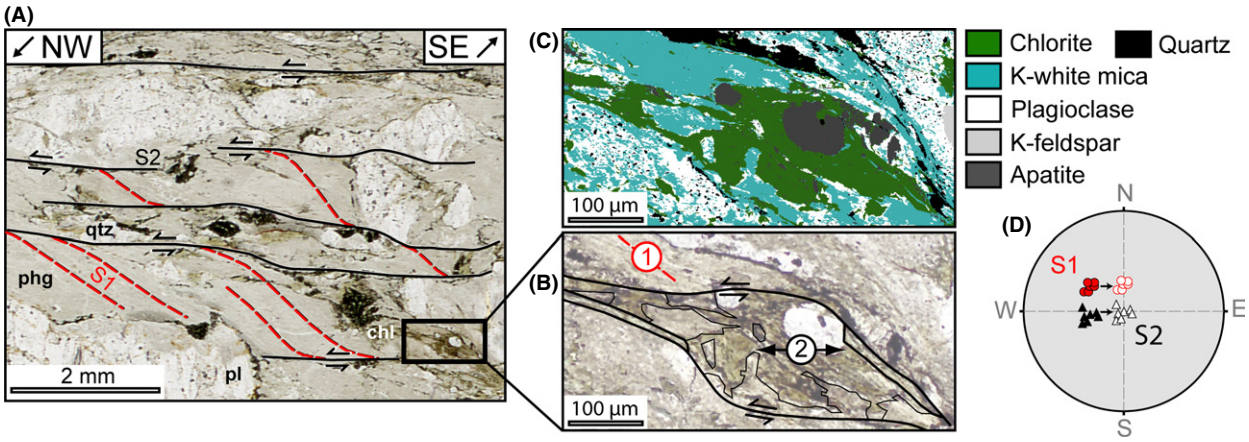

Fig. 2 Plan-de-Phasy granite sample: (A) Photomicrograph at the thin-section scale showing the two schistosities S1 (red dashed lines) and S2 (black lines). chl, chlorite; qtz, quartz; phg, phengite; pl, plagioclase. (B) Photomicrograph zoom of the mapped area. (C) Mask image in which all the pixels of the chemical map were allocated to one mineral (see Lanari *et al.*, 2013b for details). (D) Orientations of S1 (circle) and S2 (triangle) schistosity planes plotted into a Wulff diagram in lower hemisphere. Measured orientations (filled symbols) have been rotated to reconstruct the original orientation (empty symbols) before the D3 tilting event, which is related to the activity of the Durance fault (see Fig. S1).

and 300 ms dwell time (De Andrade *et al.*, 2006) and a step of 2 µm. Point analyses were measured along transects of the same area. The X-ray images were processed using the program XMapTools (Lanari *et al.*, 2013a,b). Point analyses were projected into the X-ray maps and used as internal standards for the analytical standardization. Maps of structural formulae were calculated and compositions plotted into chemical diagrams (Figs 3 and 4).

Results

Chlorite compositions show homogeneous XMg (XMg = Mg/(Mg+Fe), (Fig. 3A). Two groups of chlorite are identified from their Si contents (groups C1 with Si <3 atoms per formula unit (a.p.f.u.) in red, and C2 with Si > 3 a.p.f.u. in green in Fig. 3 respectively). C1 chlorite crystallized along S1 on the rims of the S2-related zone of fluid impregnation and outside (Fig. 3B). This textural relationship between C1 chlorite and the KWM belonging to S1 is frequently observed (Fig. 5A). In the mapped area, C2 chlorite is located in pressure shadows of apatite and between KWM fragments inside the S2-related zone of fluid impregnation (Fig. 2B, 3B). The C2 chlorite always crystallizes in pressure shadows of apatite or rutile porphyroblasts along S2 (Fig. 5B). In addition to a high Si content, C2 chlorite shows a large number of octahedral vacancies (Table 1), which is indicative of lower temperatures of crystallization (Vidal *et al.*, 2001; Grosch *et al.*, 2012).

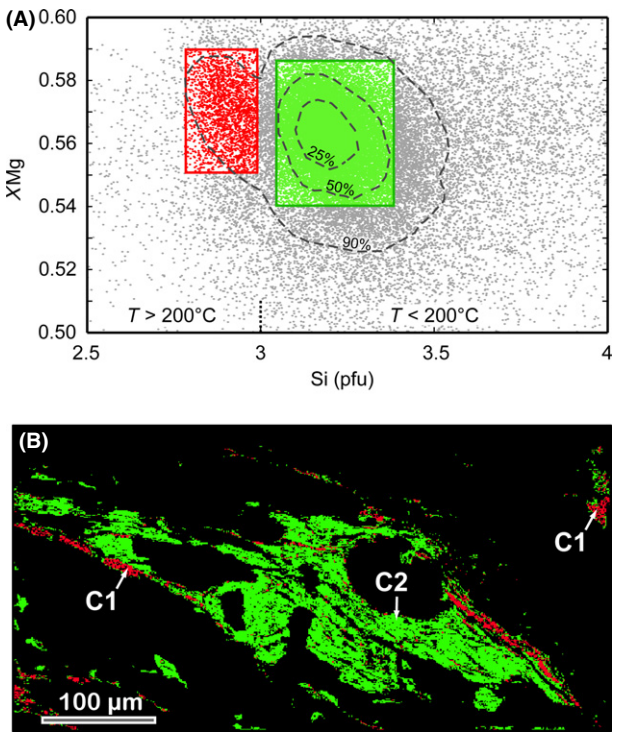

Fig. 3 Chemical analysis of chlorite. (A) All the chlorite compositions were plotted into a binary diagram of Si (atoms per formula unit) vs. XMg. The chlorite compositions were divided into two groups, C1 and C2, based on their Si content (see text for details). The dashed lines are the point density levels. (B) The corresponding pixels were plotted into a map with the same colours.

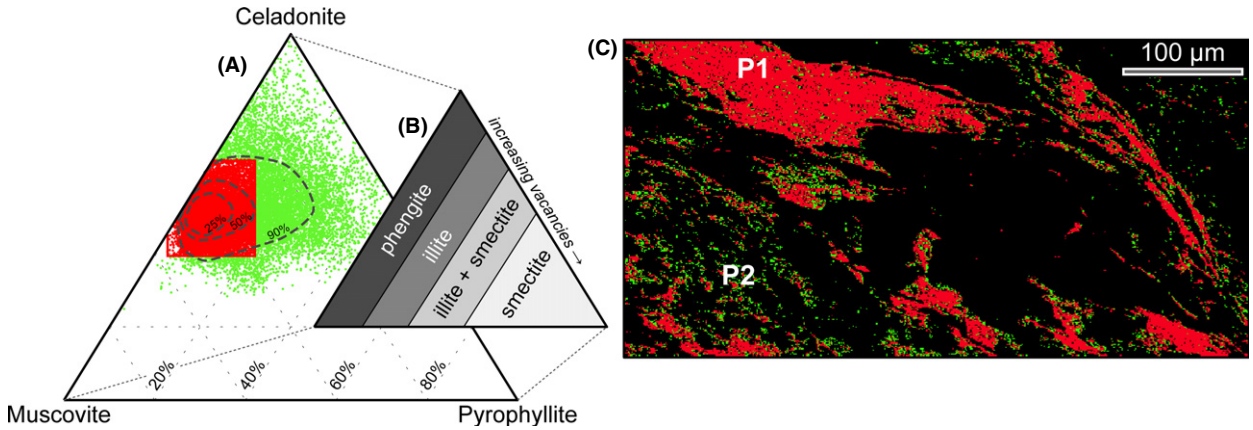

Fig. 4 Chemical analysis of KWM. (A) All the KWM compositions were plotted on a muscovite ($Si_3Al_3KO_{10}(OH)_2$), celadonite ($Si_4Al(Mg,Fe)KO_{10}(OH)_2$) and pyrophyllite ($Si_4Al_2O_{10}(OH)_2$) ternary diagram. The KWM compositions were divided into two groups, P1 and P2 (see text for details). The dashed lines are the point density levels. (B) The compositional fields of dioctahedral mica-like phases (phengite and clays) are reported on the chemical triangular diagram. (C) The corresponding pixels were plotted into a map with the same colours.

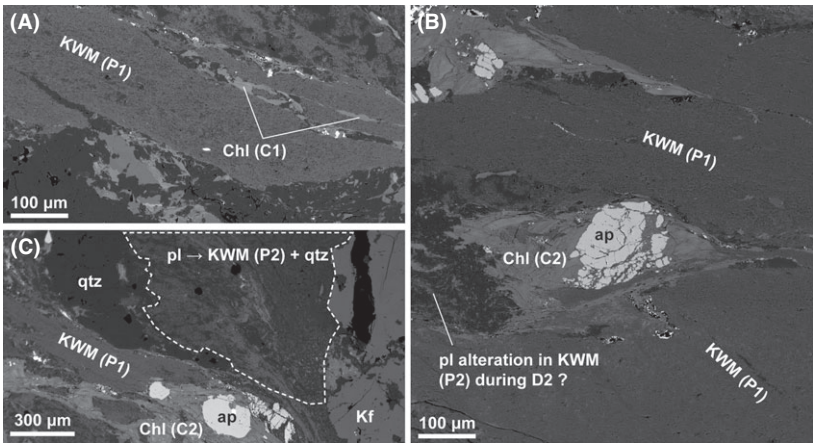

Fig. 5 BSE images of the Plan-de-Phasy granite sample. The image orientations are the same as in Fig. 2. (A) Alpine P1 phengite and C1 chlorite belonging to S1. (B) Pressure shadow of C2 chlorite growing around an apatite porphyroclast. (C) Area in which the magmatic plagioclase has destabilized in P2 to form KWM plus quartz.

KWM compositions are reported on a ternary diagram – muscovite, celadonite and pyrophyllite – and divided into two groups (Fig. 4A). The first group, P1, gathers phengite compositions with low pyrophyllite contents ((K + Na) > 0.85, Fig. 4B and Table 2), and P2 gathers illite and illite+smectite compositions with higher pyrophyllite contents [(K + Na) <0.85]. As for chlorite, the P1 and P2 groups correspond to different structural positions: P1 phengites occur in the S1 schistosity (Fig. 4C and 5), whereas P2 KWM formed from the destabilization of P1 phengite and plagioclase into KWM plus quartz (Fig. 5C). This plagioclase destabilization and the associated crystallization of the P2 KWM could be related to the D2 deformation event (Fig. 5B) or could occur during a later hydrothermal event (D3) with hot fluids following the S2 planes.

P–T estimates

The chlorite and KWM crystallization *P–T* conditions were determined using a multi-equilibrium approach. The crystallization temperatures of chlorite in equilibrium with quartz and water were estimated using the calibration of Vidal *et al.* (2006) and Inoue *et al.* (2009) for Si <3 p.f.u. and Si > 3 p.f.u. respectively. The pressure conditions were then estimated using KWM-Qtz-H_2O equilibria (Dubacq *et al.*, 2010) calculated for P1 compositions at the C1 temperatures. Temperatures and XFe^{3+} of C1 chlorite compositions were first calculated at 4, 6, 8 and 10 kbar. The KWM-Qtz-H_2O equilibrium line calculated using the average P1 KWM composition was found to intersect the C1 chlorite temperatures at 270 °C and 8.1 ± 2 kbar. At this pressure, temperatures calculated from C1 chlorites range between 240 °C and 300 °C (average temperature of 270 ± 25 °C, see Fig. 6A). The temperatures of C2 chlorites calculated with an imposed value of XFe^{3+} = 0.3 [upper value obtained for C1 chlorite with the Vidal *et al.* (2006) method] range between 100 °C and 200 °C.

Ar-Ar phengite dating

Phengite grains smaller than 500 µm were separated by hand-picking under a stereomicroscope and were irradiated for 10 h in the nuclear reactor at McMaster University (Canada) in position 5c along with Fish Canyon sanidine monitor (28.03 ± 0.08 Ma, Jourdan and Renne, 2007). The estimated errors

Table 1 Representative compositions of chlorite.

	C1-82598	C1-82047	C1-82599	C2-59162	C2-57519
CHL					
SiO_2	27.210	27.570	28.000	28.190	33.570
Al_2O_3	18.970	18.620	18.230	15.330	16.430
FeO	21.870	23.690	24.040	21.300	22.530
MnO	0.310	0.340	0.360	0.380	0.420
MgO	17.360	16.180	16.510	15.640	16.460
CaO	0.100	0.180	0.130	0.560	0.240
Na_2O	0.030	0.060	0.040	0.100	0.050
K_2O	0.170	0.130	0.140	0.210	0.410
Atom site distribution (14 Ox)					
Si (T1+T2)	2.868	2.905	2.931	3.131	3.220
Al(T2)	1.121	1.095	1.069	0.869	0.780
Al(M1)	0.121	0.095	0.069	0.000	0.000
Mg(M1)	0.490	0.463	0.482	0.491	0.482
Fe_2+(M1)	0.346	0.381	0.394	0.375	0.370
V(M1)	0.042	0.061	0.056	0.134	0.148
Mg(M2+M3)	2.237	2.078	2.095	2.025	1.747
Fe(M2+M3)	1.581	1.707	1.711	1.547	1.342
Al(M2+M3)	0.113	0.121	0.112	0.269	0.297
Al(M4)	1.000	1.000	1.000	0.869	0.780
Mg(M4)	0.000	0.000	0.000	0.074	0.125
Fe(M4)	0.000	0.000	0.000	0.057	0.095
XMg	0.586	0.549	0.550	0.566	0.567
XFe	0.414	0.451	0.450	0.434	0.433

Table 2 Representative compositions of K-white mica

	P1-120598	P1-120587	P1-120049	P2-85413	P2-85321
MICA					
SiO_2	53.14	53.07	51.46	56.18	56.15
Al_2O_3	23.14	23.58	23.93	22.24	22.18
FeO	4.22	4.42	4.29	4.14	3.92
MnO	0.04	0.04	0.05	0.04	0.04
MgO	4.55	5.01	4.24	4.15	3.72
CaO	0.07	0.05	0.05	0.09	0.1
Na_2O	0.41	0.1	0.15	0.71	1.27
K_2O	10.03	10.93	10.32	8.32	7.72
Atom site distribution (11 Ox)					
Si (T1+T2)	3.553	3.512	3.493	3.689	3.706
Al(T2)	0.447	0.488	0.507	0.311	0.294
V(M1)	0.935	0.913	0.922	0.958	0.989
Mg(M1)	0.044	0.060	0.052	0.028	0.008
Fe_2+(M1)	0.023	0.030	0.029	0.016	0.005
Al(M2+M3)	1.377	1.351	1.408	1.410	1.431
Mg(M2+M3)	0.410	0.434	0.378	0.378	0.358
Fe(M2+M3)	0.213	0.215	0.214	0.212	0.211
K(A)	0.856	0.923	0.894	0.697	0.650
Na(A)	0.053	0.013	0.020	0.090	0.163
V(A)	0.086	0.061	0.083	0.206	0.180
XMg	0.658	0.669	0.638	0.641	0.629
XFe	0.342	0.331	0.362	0.359	0.371

of the $^{40}Ar^*/^{39}ArK$ ratio range between ±0.1% (2σ) and ±0.6% (2σ) in the volume where the samples were located. Phengite grain dating was undertaken by step heating with a 50W CO_2 Synrad 48-5 continuous laser beam and the measurement of isotopic ratios was realized with a VG3600 mass spectrometer at Geoazur (detailed method in Rolland *et al.*, 2008). The two Ar-Ar spectra (Fig. 6D, Table S1) exhibit a slight staircase shape in low-temperature steps; both starting at *c.* 13 Ma. Cl/K vs. age plots (Figure S2) indicate a linear negative correlation of Cl/K with age, which argues with Cl incorporation during system reopening due to a late (<13 Ma) hydrothermal alteration event (e.g., Rolland *et al.*, 2008; Simon-Labric *et al.*, 2009). In experiment K569, a plateau is reached after the fourth step. Calculation of plateau age with the last 6 steps (comprising 55% of the released ^{39}Ar) provides an age of 45.9 ± 1.1 Ma (MSWD: 1.13), which is interpreted as a D1 crystallization age unaffected by the later system reopening. The duplicate analysis (K640) shows slightly more complex spectra with similar shape. The plateau age comprising 95% of the ^{39}Ar is similar within error to that of K569 (46.6 ± 2.6 Ma); the larger error is due to slightly older ages in the last four steps comprising only 14% of the ^{39}Ar, providing an age of 51.3 ± 0.9 Ma. This represents a minor part of the signal and is ascribed to some Ar inheritance from undetectable (<1 μm) granite protolith feldspar relicts of Hercynian age (>300 Ma). From both experiments, the main crystallization age of phengite during shear zone activity is about 46 Ma, with some partial hydrothermal reset at a maximum age of 13 Ma.

Discussion and geodynamic implications

Due to their crystallization at lower temperatures than those predicted for the closure of the K-Ar system, KWM have the potential to provide temporal constraints on their crystallization in a given geodynamic context (Warren *et al.*, 2012). Combined with detailed *P–T* data, KWM may provide useful information on the timing of exhumation, deformation (Sanchez *et al.*, 2011) and hydrothermal (Tartèse *et al.*, 2012) histories. In this study, the Alpine *P–T* peak reached by the Plan-de-Phasy unit during the D1 metamorphic event (top-to-the-N shearing event) is calculated at 270 ± 25 °C and 8.1 ±2 kbar and was dated at 45.9 ±1.1 Ma. D1 phengite grew syn-kinematically as shown by

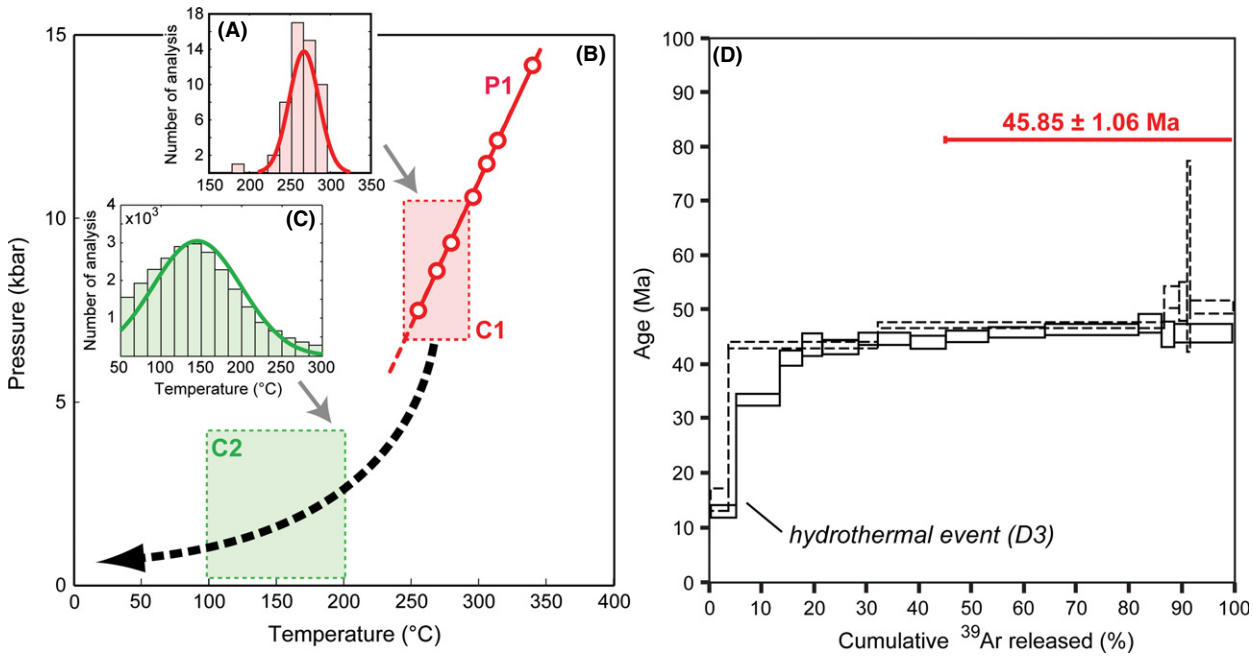

Fig. 6 *P–T–t* estimate of the metamorphic peak in the Plan-de-Phasy granite. (A) Temperatures of C1 chlorite compositions calculated using the calibration of Vidal *et al.* (2006). (B) *P–T* diagram showing the *P–T* line of phengite P1 (dots are the hydration steps) and the temperature ranges of the C1 and C2 chlorite compositions. (C) Temperatures of C2 chlorite compositions calculated using the calibration of Inoue *et al.* (2009). (D) $^{40}Ar/^{39}Ar$ spectra of P1 phengite. Age is shown at 2σ. The dashed line is the duplicate.

microtextural analyses and the lack of compositional zoning. P1 KWM grains have been locally destabilized into illite and illite+smectite clays, probably during D3. Further north, a major deformational event occurred between 34 and 30 Ma in the Pelvoux (Simon-Labric *et al.*, 2009) and at 29–30 Ma in Mont-Blanc (Cenki-Tok *et al.*, 2013), which is ascribed to underthrusting below the Briançonnais Frontal Thrust (D2 event). The low-temperature Ar loss observed in this study reflects a late (<13 Ma) alteration of KWM, probably related to hydrothermalism during the Durance normal faulting (D3), and evidenced by currently active hot springs. Such processes of hydrothermal fluid circulation are widely invoked for partial resetting of the Ar system in KWM (Tartèse *et al.*, 2011). Here, the dated grains show a first step age of 13.0 ± 1.1 Ma. This (maximum) age is in good agreement with the apatite fission-track age of 11.7 ± 1.2 obtained by Schwartz (2002) in the same unit and interpreted as partial to total annealing of the samples by hydrothermal fluids (Tricart *et al.*, 2007).

According to our results and the available *P–T–t* data in the literature, we propose to integrate the Plan-de-Phasy unit in the framework of Briançonnais Zone evolution during the Eocene (Fig. 7). At 45–50 Ma, a major D1 top-to-the-N tectono-metamorphic event corresponding to the pressure peak is recorded in the internal Briançonnais zones, in the Vanoise sedimentary cover (Gerber, 2008; Strzerzynski *et al.*, 2012) and in the Ambin gneissic basement (Ganne *et al.*, 2007). The palaeo-geothermal gradient occurring during this D1 event was calculated at 8–10 °C/km (Ganne *et al.*, 2007; Lanari *et al.*, 2012). The Plan-de-Phasy unit also recorded a top-to-the-N tectonic event at 45.9 ± 1.1 Ma along a relatively cold apparent geotherm of 11 °C/km. This unit could have been initially rooted within the Internal Briançonnais zone. The absence of any carboniferous sediment symptomatic of the 'Briançonnais zone houillère' between the Plan-de-Phasy unit basement and its Permian to Triassic sedimentary cover confirms an Internal Briançonnais origin (Fig. 7A). Assuming a convergence rate of 1.5 km Ma^{-1} during the Eocene (Handy *et al.*, 2010), we can reconstruct the geometry of the Briançonnais continental subduction at 40-37 Ma (Fig. 7B). Most of the Internal Briançonnais units were already partly exhumed by that time, except the external units such as the Briançonnais Zone Houillère (Lanari *et al.*, 2012). Exhumation of the Internal Briançonnais units resulted in scraping off the basement-cover transition while the continental subduction still continued. The HP-LT units scalped from the top of the continental slab formed a stack of continental units in front of the active continental subduction corresponding to the future Briançonnais Frontal Thrust (Fig. 7B). The final emplacement of the Plan-de-Phasy unit (Fig. 7C) in its present-day position is related to Briançonnais Frontal Thrust activity at 34-30 Ma (Simon-Labric *et al.*, 2009).

Conclusion

This study shows that it is possible to depict the tectono-metamorphic

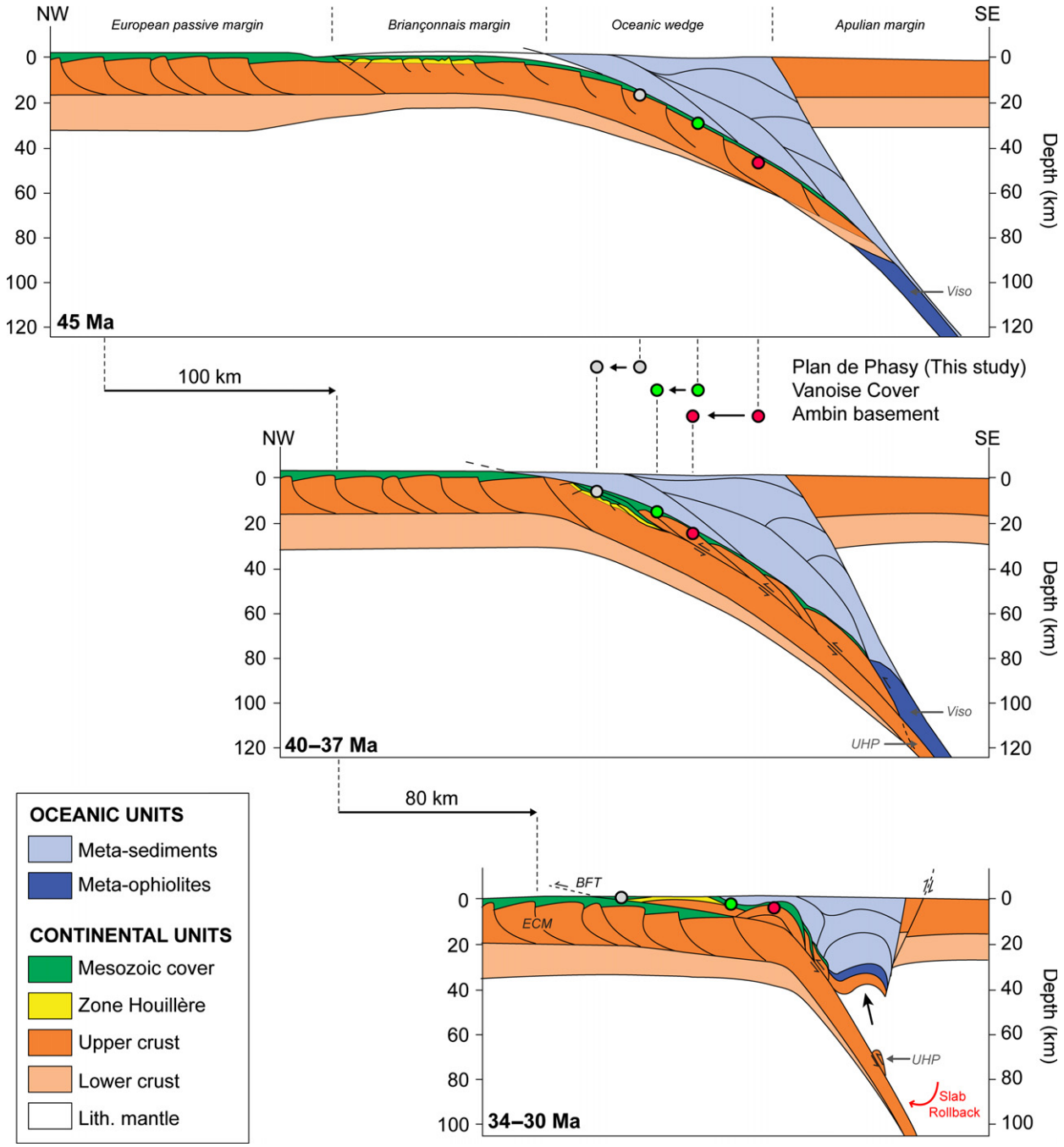

Fig. 7 Possible kinematic reconstruction of this part of the Western Alps from the Eocene to Oligocene (modified from Lanari *et al.*, 2012) including the results from this study. ECM, External Crystalline Basements; BFT, Briançonnais Front Trust

evolution of low-grade chlorite-KWM-bearing lithologies to pinpoint the main kinematic and hydrothermal events and the corresponding *P–T–t* path. Such a detailed metamorphic approach and associated geochronological study is only possible in highly deformed samples in which phengite grains are neo-crystallized, which allows a new equilibrium to be set and the K-Ar system to be completely reset. Further hydrothermal activity resulted in local mineral recrystallization and affected the Ar-Ar spectra only in their LT part.

We provide insights into the shallow activity of the Alpine subduction zone and underthrusting of Briançonnais continental crust below the so-called 'Penninic Front' at *c.* 46 Ma, which is thus distinguished from later reactivation along the Briançonnais front at 35-30 Ma corresponding to underthrusting of the External Crystalline Massifs. Further north, the two fronts are indistinguishable.

Acknowledgements

The authors acknowledge A. Pourteau (University of Potsdam) for his assistance during the electron microanalysis. S. Gallet is warmly thanked for support during Ar-Ar analysis. The article was greatly improved by constructive comments from M. Engi and three anonymous reviewers. We thank C. Doglioni for efficient editorial handling. This study was supported by the French Agence Nationale de la Recherche project no. ANR-08-BLAN-0303-01 "Erosion and Relief Development in the Western Alps", the SUBDEF grant no. ANR-08-BLAN-0192 and the Labex OSUG2020.

References

Agard, P., Monié, L., Jolivet, L. and Goffé, B., 2002. Exhumation of the Schistes Lustrés complex: in-situ laser probe $^{40}Ar/^{39}Ar$ constraints and implications for the Western Alps. *J. Metamorph. Geol.*, **20**, 599–618.

Angiboust, S., Langdon, R., Agard, P., Waters, D. J. and Chopin, C., 2012. Eclogitization of the Monviso ophiolite (W Alps) and implications on subduction dynamics. *J. Metamorph. Geol.*, **30**, 37–61.

Bousquet, R., Oberhänsli, R., Goffé, B., Wiederkehr, M., Koller, F., Schmid, S.M., Schuster, R., Engi, M., Berger, A. and Martinotti, G., 2008. Metamorphism of metasediments at the scale of an orogen: A key to the Tertiary geodynamic evolution of the Alps. In: *Tectonic Aspects of the Alpine-Dinaride-Carpathian System* (S. Siegesmund, B. Fügenschuh and N. Froitzheim, eds). *Spec. Publ. Geol. Soc. Lond*, **298**, 393–441.

Caby, R., 1996. Low-angle extrusion of high-pressure rocks and the balance between outward and inward displacements of Middle Penninic units in the western Alps. *Eclogae Geol. Helv.*, **89**, 229–267.

Cantarero, I., Lanari, P., Vidal, O., Alias, G., Travé, A. and Baqués, V., 2013. Long-term fluid circulation in extensional faults in the central Catalan Coastal Ranges: P-T constraints from neoformed chlorite and K-white mica. *Int. J. Earth Sci.* doi:10.1007/s00531-013-0963-8. In press.

Cenki-Tok, B., Darling, J. R., Rolland, Y., Dhuime, B. and Storey, C. D., 2013. Direct dating of mid-crustal shear zones with synkinematic allanite: new in situ U-Th-Pb geochronological approaches applied to the Mont Blanc massif. *Terra Nova*, **26**, 29–37.

Connolly, J.A.D., 2005. Computation of phase equilibria by linear programming: A tool for geodynamic modeling and its application to subduction zone decarbonation. *Earth Planet. Sci. Lett.*, **236**, 524–541.

De Andrade, V., Vidal, O., Lewin, E., O'Brien, P. and Agard, P., 2006. Quantification of electron microprobe compositional maps of rock thin sections: an optimized method and examples. *J. Metamorph. Geol.*, **24**, 655–668.

Dubacq, B., Vidal, O. and Andrade, V., 2010. Dehydration of dioctahedral aluminous phyllosilicates: thermodynamic modelling and implications for thermobarometric estimates. *Contrib. Miner. Petrol.*, **159**, 159–174.

Dumont, T., Schwartz, S., Guillot, S., Simon-Labric, T., Tricart, P. and Jourdan, S., 2012. Structural and sedimentary records of the Oligocene revolution in the Western Alpine arc. *J. Geodyn.*, **56–57**, 18–38.

Ernst, W. G., 1988. Tectonic history of subduction zones inferred from retrograde blueschist P-T paths. *Geology*, **16**, 1081–1084.

Gabalda, S., Beyssac, O., Jolivet, L., Agard, P. and Chopin, C., 2009. Thermal structure of a fossil subduction wedge in the Western Alps. *Terra Nova*, **21**, 28–34.

Ganne, J., Bertrand, J.M., Fudral, S., Marquer, D. and Vidal, O., 2007. Structural and metamorphic evolution of the Ambin massif (western Alps): toward a new alternative exhumation model for the Brianconnais domain. *Bulletin de la Sociéteé Geéologique de France*, **178**, 437.

Gasco, I., Gattiglio, M. and Borghi, M., 2013. Review of metamorphic and kinematic data from Internal Crystalline Massifs (Western Alps): PTt paths and exhumation history. *J. Geodyn.*, **63**, 1–19.

Gerber, W., 2008. Evolution tectono-métamorphique du Briançonnais interne: Comportement du socle et de sa couverture dans un contexte de subduction continentale profonde. University of Paris VI. 246 p.

Goffé, B., Schwartz, S., Lardeaux, J. and Bousquet, R., 2004. Explanatory notes to the map: Metamorphic structure of the alps western and ligurian alps. *Mitt. Osterr. Miner. Ges.*, **149**, 125–144.

Grosch, E.G., Vidal, O., Abu-Alam, T. and McLoughlin, N., 2012. P–T Constraints on the Metamorphic Evolution of the Paleoarchean Kromberg Type-Section, Barberton Greenstone Belt, South Africa. *J. Petrol.*, **53**, 513–545.

Handy, M.R., Schmid, S.M., Bousquet, R., Kissling, E. and Bernoulli, D., 2010. Reconciling plate-tectonic reconstructions of Alpine Tethys with the geological–geophysical record of spreading and subduction in the Alps. *Earth-Sci. Rev.*, **102**, 121–158.

Harrison, T.M., Célérier, J., Aikman, A.B., Hermann, J. and Heizler, M.T., 2009. Diffusion of ^{40}Ar in muscovite. *Geochim. Cosmochim. Acta*, **73**, 1039–1051.

Inoue, A., Meunier, A., Patrier-Mas, P., Rigault, C., Beaufort, D. and Vieillard, P., 2009. Application of Chemical Geothermometry to Low-Temperature Trioctahedral Chlorites. *Clays Clay Miner.*, **57**, 371–382.

Jourdan, F. and Renne, P., 2007. Age calibration of the Fish Canyon sanidine 40Ar/39Ar dating standard using primary K–Ar standards. *Geochim. Cosmochim. Acta*, **71**, 387–402.

Kerckhove, C. and Piboule, M., 1999. The "Plan de Phazy Granite," near Guillestre (Briançonnais zone in the Durance area of the french-italian western Alps): a hundred years old myth. *Géol. Alpine*, **75**, 117–122.

Kirschner, D.L., Cosca, M.A., Masson, H. and Hunziker, J.C., 1996. Staircase $^{40}Ar/^{39}Ar$ spectra of fine-grained white mica: Timing and duration of deformation and empirical constraints on argon diffusion. *Geology*, **24**, 747–750.

Lanari, P., Guillot, S., Schwartz, S., Vidal, O., Tricart, P., Riel, N. and Beyssac, O., 2012. Diachronous evolution of the alpine continental subduction wedge: Evidence from P–T estimates in the Briançonnais Zone houillère (France – Western Alps). *J. Geodyn.*, **56-57**, 39–54.

Lanari, P., Riel, N., Guillot, S., Vidal, O., Schwartz, S., Pêcher, A. and Hattori, K., 2013a. Deciphering High-Pressure metamorphism in collisional context using microprobe-mapping methods: application to the Stak eclogitic massif (NW Himalaya). *Geology*, **41**, 111–114.

Lanari, P., Vidal, O., De Andrade, V., Dubacq, B., Lewin, E., Grosch, E. and Schwartz, S., 2013b. XMapTools: a MATLAB©-based program for electron microprobe X-ray image processing and geothermobarometry. *Comput. Geosci.*, **62**, 227–240.

Lardeaux, J. M., Schwartz, S., Paul, A., Tricart, P., Guillot, S., Béthoux, N. and Masson, F., 2006. A crustal-scale cross section of the southwestern Alps combining geophysical and geological imagery, *Terra Nova*, **18**, 412–422.

McDougall, I. and Harrison, T. M., (1988), *Geochronology and Thermochronology by the $^{40}Ar/^{39}Ar$ Method.* New York, Oxford University Press, 212p.

Rolland, Y., Lardeaux, J. M., Guillot, S. and Nicollet, C., 2000. Extension syn-

convergence, poinçonnement vertical et unités métamorphiquescontrastées en bordure Ouest du Grand Paradis (Alpes Franco-Italiennes). *Geodin. Acta*, **13**, 133–148.

Rolland, Y., Rossi, M., Cox, S.F., Corsini, M., Mancktelow, N., Pennacchioni, G., Fornari, M. and Boullier, A.M., 2008. $^{40}Ar/^{39}Ar$ dating of syn-kinematic white mica: insights from fluid-rock reaction in low-grade shear zones (Mont Blanc Massif) and constraints on timing of deformation in the NW External Alps. In: *The Internal Structure of Fault Zones: Implications for Mechanical and Fluid-Flow Properties*(C.A.J. Wibberley, W. Kurtz, J. Imber, R.E. Holdsworth and C. Colletini, eds). *Geol. Soc. London Spec. Publ.*, **299**, 293–315.

Rolland, Y., Cox, S.F. and Corsini, M., 2009. Constraining deformation stages in brittle-ductile shear zones from combined field mapping and $^{40}Ar/^{39}Ar$ dating: the structural evolution of the Grimsel Pass area (Aar massif, Swiss Alps). *J. Struct. Geol.*, **31**, 1377–1394.

Rolland, Y., Lardeaux, J.-M. and Jolivet, L., 2012. Deciphering orogenic evolution. *J. Geodyn.*, **5**, 6–57.

Sanchez, G., Rolland, Y., Schneider, J., Corsini, M., Oliot, E., Goncalves, P., Verati, C., Lardeaux, J.-M. and Marquer, D., 2011. Dating low-temperature deformation by $^{40}Ar/^{39}Ar$ on white mica, insights from the Argentera-Mercantour Massif (SW Alps). *Lithos*, **125**, 521–536.

Schwartz, S., 2002. La zone piémontaise des Alpes occidentales: un paléocomplexe de subduction, Arguments métamorphiques, géochronologiques et structuraux. *Documents du BRGM*, **302**, 1–313.

Schwartz, S., Allemand, P. and Guillot, S., 2001. Numerical model of the effect of serpentinites on the exhumation of eclogitic rocks: insights from the Monviso ophiolitic massif (Western Alps), *Tectonophysics*, **42**, 193–206.

Schwartz, S., Tricart, P., Lardeaux, J.-M., Guillot, S. and Vidal, O., 2009. Late tectonic and metamorphic evolution of the Piedmont accretionary wedge (Queyras Schistes lustres, western Alps): Evidences for tilting during Alpine collision. *Geol. Soc. Am. Bull.*, **121**, 502–518.

Simon-Labric, T., Rolland, Y. and Dumont, T., 2009. $^{40}Ar/^{39}Ar$ dating of Penninic Front tectonic displacement (W Alps) during the Lower Oligocene (31–34 Ma). *Terra Nova*, **21**, 127–136.

Stipp, M., Stünitz, H., Heilbronner, R. and Schmid, S.M., 2002. The eastern Tonale fault zone: a 'natural laboratory' for crystal plastic deformation of quartz over a temperature range from 250 to 700°C. *J. Struct. Geol.*, **24**, 1861–1884.

Strzerzynski, P., Guillot, S., Leloup, P., Arnaud, N., Vidal, O., Ledru, P., Courrioux, G. and Darmendrail, X., 2012. Tectono-metamorphic evolution of the Briançonnais zone (Modane-Aussois and Southern Vanoise units, Lyon Turin transect, Western Alps). *J. Geodyn.*, **56-57**, 55–75.

Tartèse, R., Boulvais, P., Poujol, M., Chevalier, T., Paquette, J.-L., Ireland, T.R. and Deloule, E., 2012. Mylonite of the South Armorican Shear Zone: Insights for crustal-scale fluid flow and water-rock interaction processes. *J. Geodynm.*, **65-66**, 86–107.

Tartèse, R., Ruffet, G., Poujol, M., Boulvais, P. and Ireland, T.R., 2011. Simultaneous resetting of the muscovite K-Ar and monazite U-Pb geochronometers: a story of fluids. *Terra Nova*, **23**, 390–398.

Tricart, P., 1984. From passive margin to continental collision – a tectonic scenario for the Western Alps. *Am. J. Sci.*, **284**, 97–120.

Tricart, P. and Schwartz, S., 2006. A north-south section across the Queyras Schistes lustrés (Piedmont zone, Western Alps): Syn-collision refolding of a subduction wedge. *Swiss J. Geosci.*, **99**, 429–442.

Tricart, P., Bouillin, J.P., Dick, P., Moutier, L. and Xing, C., 1996. Le faisceau de failles de haute-Durance et le rejeu distensif du front briançonnais au SE du Pelvoux (Alpes occidentales). *C. R. Acad. Sci. Paris*, **323**, 251–257.

Tricart, P., van der Beek, P., Schwartz, S. and Labrin, E., 2007. Diachronous late-stage exhumation across the western Alpine arc: constraints from apatite fission-track thermochronology between the Pelvoux and Dora-Maira. *J. Geol. Soc. London*, **164**, 163–174.

Vidal, O. and Parra, T., 2000. Exhumation paths of high-pressure metapelites obtained from local equilibria for chlorite–phengite assemblages. *Geol. J.*, **35**, 139–161.

Vidal, O., Parra, T. and Trotet, F., 2001. A thermodynamic model for Fe–Mg aluminous chlorite using data from phase equilibrium experiments and natural pelitic assemblages in the 100–600 °C 1–25 kbar range. *Am. J. Sci.*, **63**, 557–592.

Vidal, O., De Andrade, V., Lewin, E., Munoz, M., Parra, T. and Pascarelli, S., 2006. P-T-deformation-Fe^{3+}/Fe^{2+} mapping at the thin section scale and comparison with XANES mapping: application to a garnet-bearing metapelite from the Sambagawa metamorphic belt (Japan). *J. Metamorph. Geol.*, **24**, 669–683.

Warren, C.J., Hanke, F. and Kelley, S.P., 2012. When can muscovite $^{40}Ar/^{39}Ar$ dating constrain the timing of metamorphic exhumation? *Chem. Geol.*, **291**, 79–86.

Received 28 January 2013; revised version accepted 11 October 2013

Supporting Information

Additional Supporting Information may be found in the online version of this article:

Fig. S1. Structural sketch and evolution of the Plan-de-Phasy unit. (i) Panorama view of the «écailles de Plan de Phasy» area between Plan de Phasy and Saint Clément, view is towards the south. (ii) Detailed view of the Plan-de-Phasy granite and the surrounding units. (iii.1) Plan-de-phasy unit block diagram. (iii.2) Triassic limestone block diagram. (iv) Table showing the deformation history of the Plan-de-Phasy unit.

Fig. S2. Cl/K versus $^{40}Ar/^{39}Ar$ age plot of KMW from mylonitized granite collected in the Plan-de-Phasy shear zone.

Table S1. $^{40}Ar/^{39}Ar$ isotopic data for phengite from the Plan-de-Phasy granite sample. Units in the different Ar isotopes are given in volts.